Polarization-dependent water adsorption on the $LiNbO_3$(0001) surface

S. Sanna,* R. Hölscher, and W. G. Schmidt
Lehrstuhl für Theoretische Physik, Universität Paderborn, 33095 Paderborn, Germany
(Received 25 August 2012; revised manuscript received 8 October 2012; published 5 November 2012)

The effect of ferroelectric poling on the adsorption characteristics of water at lithium niobate surfaces is investigated by *ab initio* calculations. Thereby we model the adsorption of H_2O monomers, small water clusters, and water thin films on the $LiNbO_3$(0001) surface. The adsorption configuration and energy are determined as a function of the surface coverage on both the positive and negative (0001) surfaces. Confirming the results of temperature programed desorption measurements [Garra, Vohs, and Bonnell, Surf. Sci. **603**, 1106 (2009)], polarization-dependent adsorption energies, geometries, and equilibrium coverage are found. Our calculations predict the adsorption to occur mainly nondissociatively, independently of the coverage. The water structures formed at the surface are coverage-dependent, though. The different affinity of water to the two surfaces is explained in terms of electrostatic interactions between the substrate and polar molecules. Water adsorption accentuates the surface relaxation, thus increasing the microscopic surface roughness.

DOI: 10.1103/PhysRevB.86.205407 PACS number(s): 68.43.Bc, 68.08.De, 82.30.Rs

I. INTRODUCTION

Lithium niobate [$LiNbO_3$ (LN)] is one of the most important optic materials because it is the equivalent in the field of nonlinear optics and optoelectronics to silicon in the field of electronics.[1] Because of its unusual and favorable optical, piezoelectric, pyroelectric, electro-optic, elastic, photoelastic, and photorefractive properties, LN is frequently used for various (nonlinear) optical and acoustic applications.[2] Furthermore, the possibility of switching the internal spontaneous polarization paves the way for the realization of ferroelectric memory devices.[3] While traditional applications mainly exploit LN bulk properties, more recently the (microscopic) surface and interface properties have become important.[4] In particular, the polarization domains of ferroelectric oxide surfaces can be manipulated by an external electric field in order to tailor the surface reactivity for specific applications. Indeed, polarization-dependent physical and chemical surface phenomena have been reported. Surface conductivity,[5] threshold energy for photoelectron emission,[6] thermally stimulated electron emission,[7] and the etching rate in acid solutions[8,9] have been shown to be very different for differently polarized domains. Polarization-dependent adsorption of particle and molecules, either directly on the ferroelectric surface[10,11] or on metal and semiconducting thin films deposited in a ferroelectric support,[12] have been demonstrated too.

In addition, photochemical deposition reactions can be combined with the local control of the ferroelectric polarization to drive the assembly of surface nanostructures.[13] Thus, domain engineering paves the way for the realization of molecular detectors and other devices at the nanoscale level. In fact, it has been suggested that molecular adsorption may stabilize opposite poling directions in ferroelectric thin films, allowing for the realization of ferroelectric chemical sensors.[14]

Due to these interesting possibilities, different studies have been dedicated to an understanding of the mechanisms behind the polarization-dependent interaction between adsorbates and surfaces. These include the photochemical deposition of metal nanoparticles,[15,16] deposition of charged particles,[17] and the adsorption and reaction of molecules on different ferroelectric surfaces.[10,18,19] These studies yield a rather complicated picture, in which many factors such as internal and external screening charges on the surfaces, electrostatic forces induced by space-charge layers and band bending, pyroelectric and piezoelectric effects, as well as charge transfer processes contribute to the observed polarization dependence of the adsorption. These contributions depend, in turn, on the particular ferroelectric surface (electronic carrier density, electronic band gap, the presence of defects, and domain boundaries), on its preparation (sample thickness, polishing, and annealing temperature), and on the experimental setup (substrate temperature, environment composition and pressure, and light source used for the carrier excitation).

Water molecules have a prominent position among the common adsorbates because of their role in natural phenomena such as catalysis, electrochemistry, and corrosion, and because of a variety of applications, including hydrogen production, fuel cells, and biological sensors. Furthermore, water will be present and influence the performance of the LN-based devices unless they operate in ultrahigh vacuum (UHV). The functionality of devices operating in particular environments might even depend on the relative humidity. Indeed, water temperature programed desorption (TPD) measurements at the positive and negative surface of $LiNbO_3$ indicate that the molecule-surface interaction is both coverage- and polarization-dependent. Another reason to study the water-LN interface is related to the fact that up to now, high-resolution atomic force images of the LN surface could only be obtained in a liquid environment.[20] To understand the experimental observations, we study the coverage-dependent adsorption of water at the positive and negative LN(0001) surface by means of atomistic simulations in the framework of the density functional theory (DFT). Adsorption energy, site, and configuration are determined, and the bond between water and surface is analyzed and discussed. Surface thermodynamics is used to predict the ground state of water-covered LN surfaces in dependence on temperature and pressure.

II. METHODOLOGY

Total energy density functional calculations have been performed within the PW91 formulation of the generalized

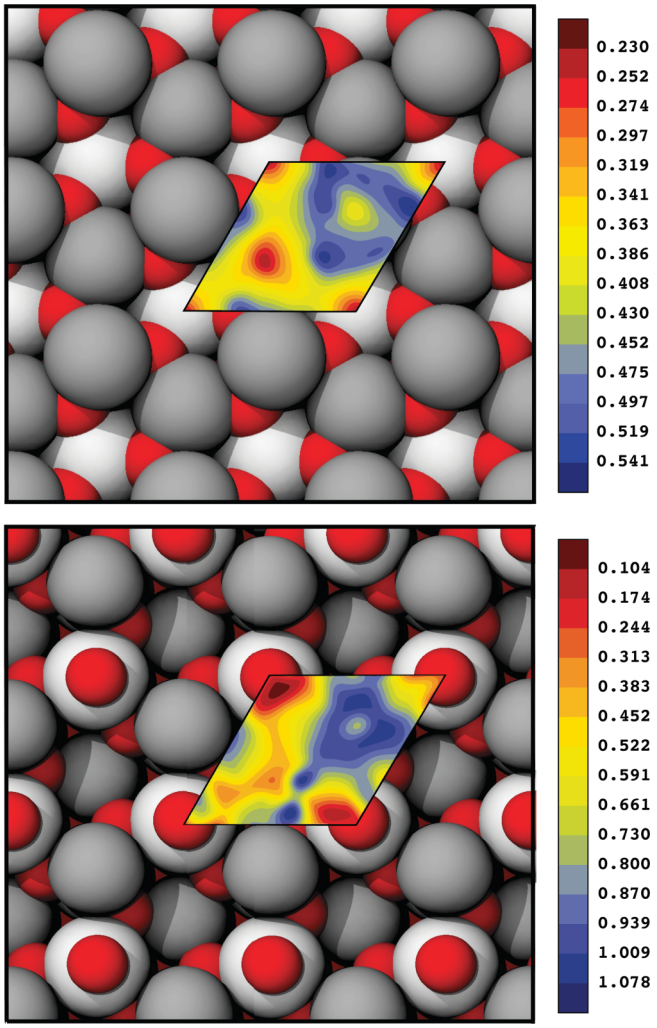

FIG. 1. (Color online) PES for the adsorption of a single H_2O molecule on the positive (upper picture) and negative (lower picture) LN(0001) surface. Li atoms are gray, Nb white, and oxygen red. Adsorption energies are in eV.

gradient approximation (GGA)[21] as implemented in the VASP simulation package.[22] The GGA functional has been shown to be crucial for the accurate treatment of hydrogen bonds and water structures[23] and to yield reliable structures and energies for both LN bulk and surfaces.[24,25] Projector augmented wave (PAW) potentials[26] with projectors up to $l = 3$ for Nb, $l = 2$ for Li and O, and $l = 1$ for H have been used for the calculations. The electronic wave functions are expanded into plane waves up to a kinetic energy of 400 eV.

The stoichiometry and the morphology of differently polarized LN clean surfaces are known to be different.[25,27–30] Our work is based on the stable surface models proposed in Refs. 25 and 29, which are in agreement with the experimental observation. According to these models, the positive surface is -Nb-O_3-Li_2 terminated, with one of the two top Li atoms relaxing down to the lower-lying oxygen layer and the other above it, as represented in Fig. 1(a). The negative surface is -Li-O terminated instead [see Fig. 1(b)]. These models are used as a basis for the investigation of the H_2O adsorption. Thereby, we use slabs consisting of 18 atomic layers within a 2×2 periodicity (124 atoms for the positive face and 128 for the negative) and a vacuum region of ∼16 Å. The lateral dimension of the unit cell largely reduces the unwanted interactions between the adsorbates and their periodic images. Using one molecule per slab corresponds, in a first approximation, to the zero-coverage adsorption (or desorption) investigated, for example, in Ref. 11. In our work, the slabs are handled in strict adherence to the approach described in Ref. 25. Following this approach, the ions of the side that is not investigated are kept frozen at their bulk positions. We have performed several test calculations with slabs containing the stable termination at each side. These tests confirm the obtained results within the numerical accuracy of the method. The dipole correction described in Refs. 31 and 32 has been used to correct the artificial forces generated by the slab images. A Γ-centered $2 \times 2 \times 1$ k-point mesh was used to carry out the integration in the Brillouin zone. The adsorbate and the six uppermost surface layers were allowed to relax until the forces acting on each atom were lower than 20 meV/Å.

III. RESULTS

We started our investigation with a determination of the favored adsorption site for single H_2O molecules on the considered model structure. We follow Refs. 2, 25, and 29 concerning the convention for discriminating positive and negative surfaces, which differs from Ref. 11. Due to the complexity and low symmetry of the LN (0001) surface, it is not sufficient to simulate the adsorption of water monomers on a few high-symmetry points (typically top, bridge, hollow, etc. for hexagonal structures). In a first step, we have therefore calculated the potential energy surface (PES) for single adsorbates, which gives an approximate idea of the stable adsorption sites and a map of the different energy minima on the surface. The PES is calculated constraining the lateral coordinates of the oxygen atom of the adsorbate and allowing the remaining degrees of freedom and the uppermost six substrate layers to relax. We have evaluated the adsorption energy for 48 possible positions and three different starting configurations, namely with the water dipole moment parallel, antiparallel, and perpendicular to the spontaneous polarization of the substrate. The results are reported in Figs. 1(a) and 1(b) for the adsorption at the positive and negative side, respectively. The PESs are relatively corrugated, indicating a low surface mobility of the adsorbate. This holds in particular for the negative surface. Several minima and maxima of the adsorption energy are present at both sides. As a general feature, H_2O avoids a position right on top of the topmost Li atoms, and it prefers an adsorption site between cations, above the lower-lying oxygen atoms (second oxygen layer from the surface top).

A. Zero-coverage adsorption

In a second step, we have determined the optimal configuration for the adsorption at both (0001) sides. Thereby, we start with the adsorbate in several of the favored adsorption sites as obtained from the PES calculation. However, we now let the molecule and the surface relax without any constraints. The water molecules do not move considerably toward other

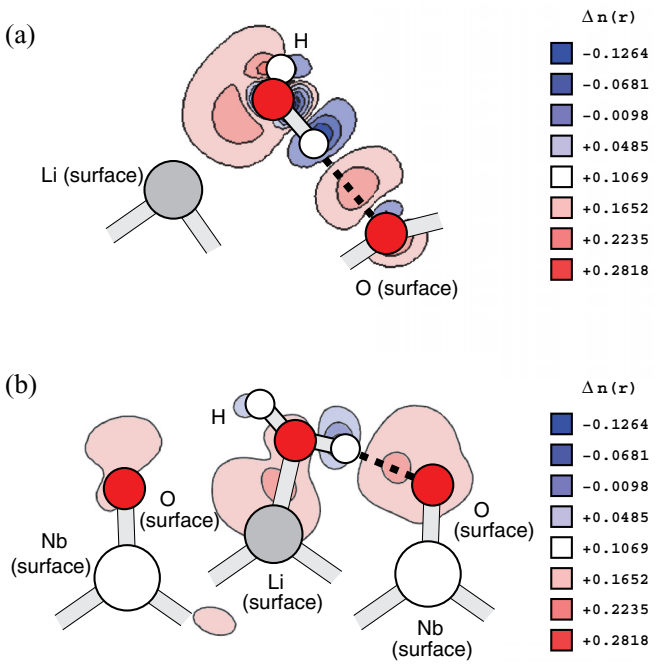

FIG. 2. (Color online) Charge redistribution upon adsorption of the H_2O molecule at the positive (a) and negative (b) (0001) surface. Charge isolines in the $(1\bar{1}00)$ plane (which is the y plane as defined in 25) are plotted. This plane contains the two bonds formed by the water molecule with the LN surface. In red are regions in which electronic charge is accumulated, in blue are regions of electronic charge depletion.

adsorption sites, indicating that the mesh used for the PES calculation was dense enough.

In the energetically favored configuration, the water molecule adsorbs quite tilted on the positive surface [see Fig. 2(a)] between one Li and one oxygen of the surface, with atomic distances $d(\mathrm{O}-\mathrm{Li}) = 2.06$ Å and $d(\mathrm{O}-\mathrm{H}) = 1.76$ Å. Both the Li-O and O-H-O directions lie in the $(1\bar{1}00)$ plane. The water adsorption at the positive side does not substantially affect the substrate geometry. An analysis of the charge density reveals a polarization cloud between a water hydrogen and the surface oxygen it points to, as well as the negative charge accumulation at the oxygen side between molecule and surface Li [see Fig. 2(a)]. The charge distribution, the interatomic distances,[33] and the adsorption geometry suggest that water molecules form both a Li-O bond of ionic character and a hydrogen bond at the positive surface.

In the case of the negative surface, the oxygen of the water molecule adsorbs close to a surface Li, at a distance $d(\mathrm{O}-\mathrm{Li}) = 1.83$ Å. One of the two hydrogen atoms points to a neighboring surface oxygen, with distance $d(\mathrm{O}-\mathrm{H}) = 1.50$ Å, while the other points out from the surface, as represented in Fig. 2(b). Charge distribution, interatomic distances, and geometry are compatible with a Li-O bond and an O-H hydrogen bond. The presence of the adsorbate induces some relaxation of the surface atoms. The adsorption pulls the surface Li out of its relaxed surface position and elongates its three bonds to neighboring oxygen ions. This is very similar to the effect of water adsorption at the nonpolar $Al_2O_3(0001)$ surface, which was recently found to significantly disrupt the clean Al_2O_3 surface geometry.[34] We notice that another configuration of very similar energy can be created. In this case, the oxygen of the water molecule again adsorbs close to a surface Li, at a distance $d(\mathrm{O}-\mathrm{Li}) = 1.89$ Å. However, both hydrogen atoms point roughly to a neighboring oxygen, with distances $d(\mathrm{O}_1-\mathrm{H}) = 1.88$ Å and $d(\mathrm{O}_2-\mathrm{H}) = 2.16$ Å. In this second configuration, all the water atoms are bound to the surface, with an ionic Li-O bond and two O-H hydrogen bonds (of different strength). In all the stable configurations, the z component of the molecular dipole moment is directed against the spontaneous polarization of the substrate, thus reducing the total polarization.

The adsorption energy, as calculated from the difference

$$E_{\mathrm{ads}} = E_{\mathrm{slab}}(\mathrm{H_2O@LN}) - E_{\mathrm{slab}}(\mathrm{LN}) - E_{\mathrm{gas}}(\mathrm{H_2O}), \quad (1)$$

amounts to 0.61 and 1.28 eV for the adsorption at the positive and negative surface, respectively. The calculated energy difference is in qualitative agreement with the TPD measurements of Garra *et al.*[11] However, the measured adsorption energy difference (estimated to be between 2.8 and 4.0 kJ/mol, corresponding to 0.029–0.041 eV) is lower than the values predicted by the theory (0.67 eV) by one order of magnitude. This discrepancy may partially be explained by the relatively large error bars affecting both the measurements and the calculations. At one side, the experimental value is obtained modeling the TPD spectra within the Polany-Wigner relations, which contain preexponential factors to be determined, and for which values scattered over several orders of magnitude have been reported (see Ref. 11 for a detailed explanation of the procedure). It is also not clear to what extent the experimental preparation conditions result in the (thermodynamically stable) surface atomic structures supposed in our study. From a theoretical point of view, it has to be said that adsorption energies do strongly depend on the parametrization of the exchange-correlation functional, both directly and indirectly through their geometry dependence. Due to these limitations, the qualitative agreement between theory and experiment achieved in the present work may be considered to be satisfactory. We mention that a recent theoretical study[35] on the adsorption of methanol on lithium niobate Z-cut surfaces also found larger adsorption energy differences between a positive and negative surface than were concluded from the experimental data. The sizable adsorption energy difference calculated in this work can be understood from an atomistic and an electrostatic perspective. The disparity of the values can be traced back to the different bonding scenario at the two sides. The bond at the negative side is shorter, i.e., stronger than at the positive surface. This is due, in turn, to the different stoichiometry and morphology of the two (0001) sides. From an electrostatic perspective, it must be considered that the work function at the positive side is larger by about 2 eV than at the negative side.[6,25] This could contribute to the difference in adsorption energy by affecting the electron transfer between the molecule and the surface, thus explaining why the H_2O adsorption at the negative side is favored with respect to the adsorption at the positive side. We remark that Garra *et al.*[11] give an alternative explanation for the observed values. According to their model, the shift in desorption temperature is caused by a difference of a few

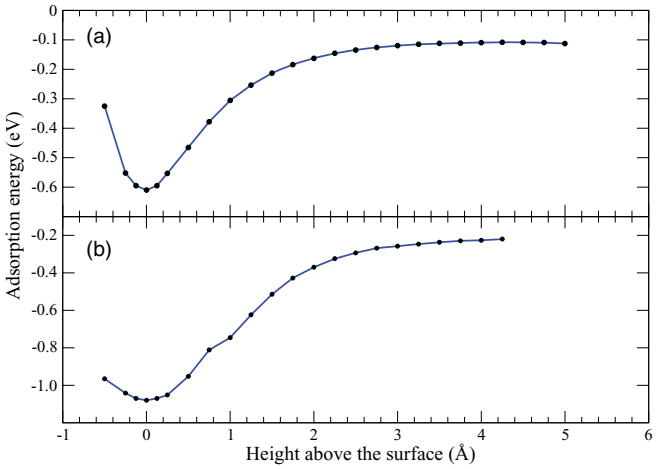

FIG. 3. (Color online) Adsorption energy (in eV) as a function of the molecule-surface distance. The equilibrium position is the scale zero. (a) Positive surface, (b) negative surface.

kJ/mol in the zero-coverage desorption energy. The authors trace this effect back to an electrostatic interaction between adsorbates (specifically, the hydrogen atoms in water) and excess screening charge due to the pyroelectric effect.

We have investigated the adsorption energy in dependence on the molecule-surface distance in order to find out whether the water molecules have to overcome an energy barrier to adsorb at the LN surface (and in this case determine its magnitude). Thereby, starting with the favored adsorption configuration, the oxygen ion of the water molecule is rigidly translated upward (perpendicular to the surface), while the rest of the system (including the six uppermost surface layers) is free to relax. The calculated adsorption energy is represented in Fig. 3. Both for the positive and the negative surface, the height-dependent adsorption energy is a monotonically increasing function of the distance from the surface, until the saturation value (represented by the gas phase) is reached. Water molecules can adsorb in their minimum energy positions at the LN(0001) without any energy barrier.

B. Higher coverages

Depending on the experimental conditions, surface adsorbed water may form different low-dimensional structures, ranging from isolated monomers and clusters to one-dimensional (1D) chains and a two-dimensional (2D) overlayer (see, e.g., Ref. 36). With increasing coverage, water may form networks of hydrogen-bonded molecules, water multilayers, and bulk icelike structures. To study the water adsorption at higher coverage, we systematically increased the number of water molecules up to four per surface unit cell. Different adsorption configurations as well as (partially) dissociated adsorption models were probed. All the tentative model structures are surface-commensurate, even for higher coverage. No long-range water reconstructions (i.e., larger than a 2×2 repetition of the unit cell) have been investigated. A number of different structures have been found to be (meta)stable; the most relevant among them are shown in Figs. 4 and 5. At the positive surface, with two water molecules per unit cell, both highly regular honeycomb structures (similar

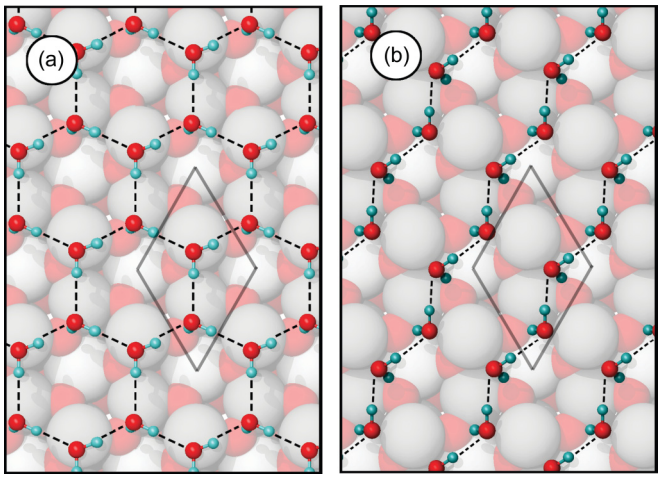

FIG. 4. (Color online) Possible water configurations at the positive (0001) surface include (a) two-dimensional regular hexagonal structures and (b) chains. The rhombohedral unit cell is highlighted.

to the water hexagons formed on many metal oxide or metal surfaces[34,37]) or water chains [as observed on rutile or ZnO (Ref. 38)] have been found. They are shown in Figs. 4(a) and 4(b), respectively. In both configurations, the water hydrogen atoms point alternatingly to a surface oxygen and to the oxygen atom of the next water molecule. Three molecules per unit cell lead to the formation of a slightly distorted form of hexagons or chains plus an isolated water monomer. Four or more molecules per unit cell give rise to three-dimensional icelike structures. The most stable of them is reminiscent of regular ice, Ih.

The negative (0001) surface is by far not as flat as the positive surface. It is rather characterized by a stronger surface corrugation. This hinders the uniform and regular adsorption of water films in regular patterns, as in the case of the positive surface. Most of all, no more than two water molecules per unit cell can be adsorbed. Increasing the number of water molecules results in the formation of ice layers separated from the surface (negative adsorption energy). Among the stable

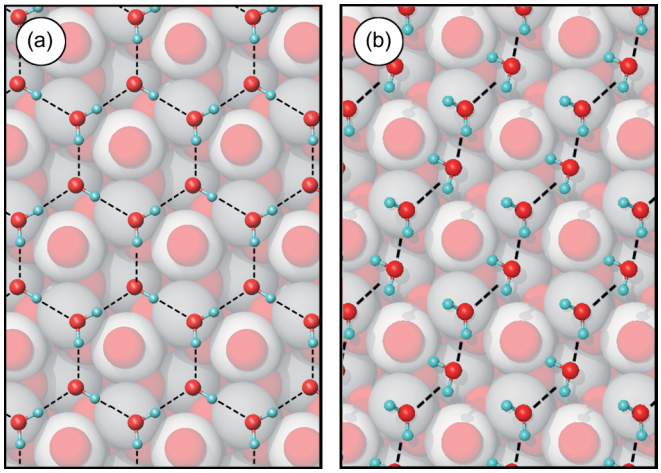

FIG. 5. (Color online) Possible water reconstructions at the negative (0001) surface include two-dimensional (a) hexamer structures and (b) less regular chain structures.

structures, honeycomb films and different kinds of distorted hexamers can be formed, as shown in Fig. 5. The dotted lines joining the water molecules are arbitrarily drawn guides for the eye and do not represent a chemical bond. We remark that our adsorption models are based on ideal surfaces created in vacuum. Real surfaces will be characterized by steps, and other surface defects (primarily oxygen and Li vacancies) will be characterized by the presence of other adsorbates and, in the case of extremely O-rich growth conditions, even by a different termination.

The particular water structure occurring on the LN surface depends on the water availability. To compare different surface water structures energetically, we use the thermodynamic grand-canonical potential:

$$\Omega(\mu^{H_2O}) = F(n) - n\mu^{H_2O} \approx E(n) - n\mu^{H_2O}. \quad (2)$$

In this equation, n is the number of water molecules and $F(n)$ is the free energy of a surface with n adsorbed water molecules. In our work, the free energy is approximated by the DFT total energy $E(n)$, which is a reasonable approximation if we assume similar entropy contributions for different adsorption configurations.[39] The formation energy of the different water structures in dependence on the water chemical potential μ^{H_2O} is plotted in Fig. 6. The chemical potential μ^{H_2O} represents the water availability. Extreme water-rich conditions are marked by a vertical line labeled $\mu^{[ice]}_{H_2O}$. This value corresponds to $LiNbO_3$ surfaces in equilibrium with bulk water approximated here by calculations for ice Ih.[40] When the water chemical potential decreases, the environment becomes dryer until the value $\mu^{[gas]}_{H_2O}$ is reached. At this value, $LiNbO_3$ surfaces are in equilibrium with water in the gas phase. The structure with the lowest formation energy, represented in the phase diagram by the lowest segment, will be formed at each value of μ_{H_2O} For an absolutely dry environment, the clean $LiNbO_3$ surface is stable. As the environment gets more and more humid, a variety of water-adsorbed surface structures may be observed. Interestingly, for intermediate conditions, the structure consisting of regular hexagons is favored upon the adsorption of isolated molecules at the positive side. This indicates that not only the water-surface interaction but also the interwater hydrogen bonding plays an important role in the formation of surface structures. At the same intermediate conditions, isolated water monomers are favored at the negative surface instead. This is probably due to the rugged morphology of the surface, which hinders the uniform and regular adsorption of water films in regular patterns. Finally, for water-rich conditions, 3D water structures (i.e., bulk ice) will be formed at both sides. Regular ice Ih structures are formed upon adsorption of more than four water molecules per surface unit cell. Thereby, the first water layer at the ferroelectric-ice interface shows a relatively regular honeycomb pattern, irrespective of the polarization direction.

The chemical potential can be directly related to the experimental conditions. In the following, $\Delta\mu_{H_2O}$ refers to the difference between the water chemical potential μ_{H_2O} and its value in the ice phase $\mu^{[ice]}_{H_2O}$. The dependence of $\Delta\mu_{H_2O}$ on temperature and pressure can be calculated in the approximation of a polyatomic ideal gas[41] as

$$\Delta\mu_{H_2O}(p,T) = k_B T\left[\ln\left(\frac{pV_Q}{k_B T}\right) - \ln Z_{rot} - \ln Z_{vib}\right], \quad (3)$$

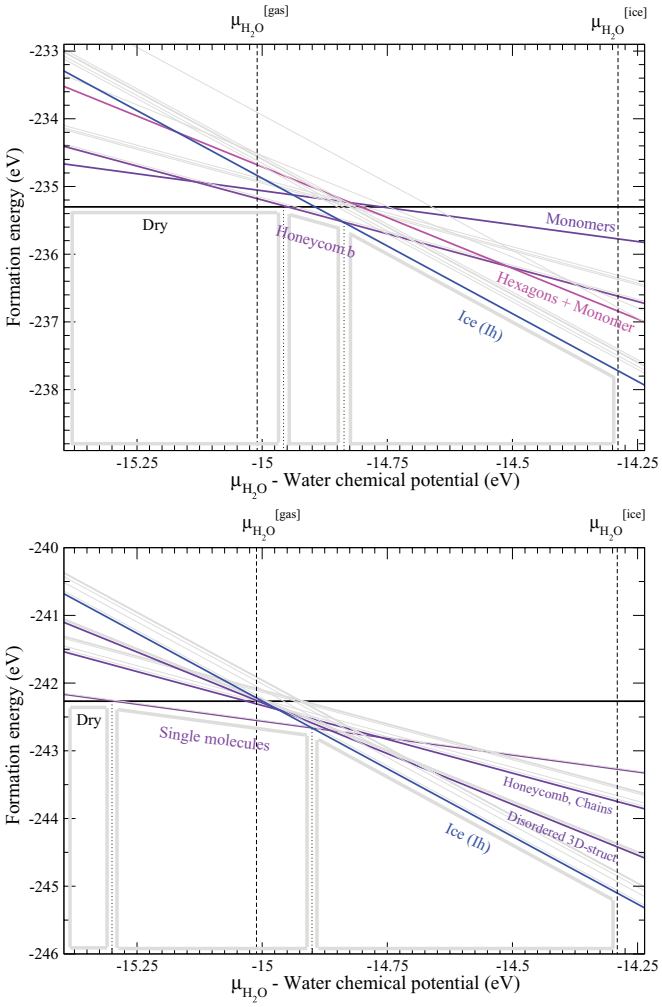

FIG. 6. (Color online) Calculated phase diagram of the positive (a) and negative (b) $LiNbO_3$(0001) surface as a function of the water availability. The latter is represented by the water chemical potential μ^{H_2O}. Two representative values of μ^{H_2O}, corresponding to water in gas (ideal gas, i.e., noninteracting molecules) and solid (ice Ih) states, are indicated. Between the two values, the water availability changes continuously, whereby the water chemical potential is at each point in equilibrium with the $LiNbO_3$ surface.

where k_B is the Boltzmann constant, T is the temperature, and p is the pressure. V_Q is the quantum volume and is equivalent to λ^3, whereby λ is the de Broglie thermal wavelength of the water molecule:

$$\lambda = \sqrt{\frac{2\pi\hbar^2}{mk_B T}}. \quad (4)$$

In this equation, m represents the mass of the H_2O molecule, and

$$Z_{rot} = \frac{(2k_B T)^{\frac{3}{2}}(\pi I_1 I_2 I_3)^{\frac{1}{2}}}{\sigma\hbar^3}, \quad (5)$$

$$Z_{vib} = \prod_\alpha \left[1 - \exp\left(-\frac{\hbar\omega_\alpha}{k_B T}\right)\right]^{-1} \quad (6)$$

are the the rotational and vibrational partition functions, respectively. We used the experimental values of the momenta of inertia I_i and of the vibrational frequencies ω_α of the

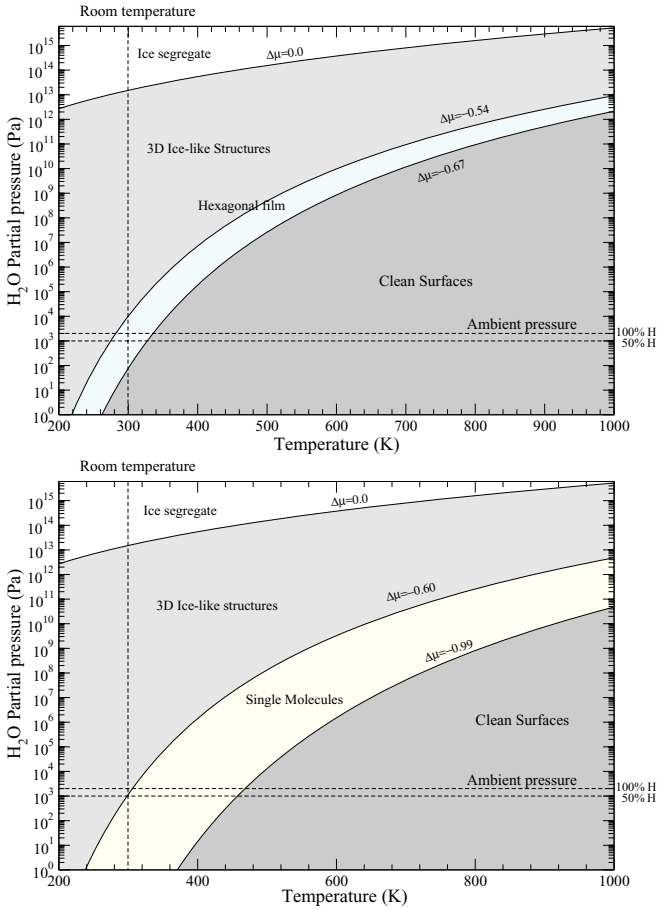

FIG. 7. (Color online) Calculated phase diagram of the positive (upper part) and negative (lower part) $LiNbO_3$(0001) surface as a function of the temperature and pressure. Dotted lines indicate the ambient conditions. The values of the chemical potential variations $\Delta\mu^{H_2O}$ (given with respect to ice *Ih*) at which a particular structure is formed are indicated by solid lines.

water molecule.[42] The geometrical parameter σ takes the symmetry of the molecule into account. For H_2O (equal-sided triangle), it holds that $\sigma = 2$. The calculated phase diagram of H_2O at the positive LN(0001) surface as a function of pressure and temperature is shown in Fig. 7 (top). According to our calculations, a water film with hexagonal symmetry is present at the LN surface at ambient condition with a relative humidity of about 50%. This is not surprising, as the adsorption of polar molecules is known to be the major external charge-compensation mechanism.[43] Heating the system above 100 °C, clean LN (i.e., water-free) surfaces are recovered. Increasing the water partial pressure above the room pressure yields the growth of water bilayers and 3D structures. At the negative side (Fig. 7, lower part), water monomers or ice seeds are present at ambient conditions. Our calculations predict a very interesting behavior: according to the phase diagrams in Fig. 7, water shall freeze at different temperatures on differently polarized LN surfaces. Indeed, this phenomenon has been experimentally observed recently for the isostructural ferroelectric $LiTaO_3$.[44]

Garra *et al.* have proposed that water adsorbs on the LN surfaces through a bonding interaction between each molecule's oxygen and a surface cation (Li,Nb), as well as through the electrostatic interaction between the molecule's hydrogen atoms and oxygen atoms on the surface.[11] Our microscopic calculations clearly confirm and validate this model. In qualitative agreement with the experiment, the relative adsorption energy per water molecule decreases with the water coverage. The energetic difference between adsorption geometries is, however, smaller than 15%. This indicates that the surface-molecule interaction is dominant over the molecule-molecule interaction. In further agreement with Ref. 11, the water adsorption is found to occur mainly nondissociatively. To investigate this behavior, the total energy of dissociated water molecules has been calculated in 30 different configurations at each side. Thereby, water fragments have been posed at the stable adsorption sites for O and OH radicals as calculated in Ref. 45. At both sides, the molecular adsorption was favored over the dissociated adsorption by at least 0.02 eV. This difference is, however, comparable with the accuracy of the approach. Thus, dissociative adsorption cannot be excluded. More generally, the presence of different adsorbates in the atmosphere could modify the thermodynamic stability of the surfaces and favor dissociative adsorption. Furthermore, dissociative adsorption might occur close to a surface defect or in the vicinity of a step, as in the case of MgO(100) and other metal oxide surfaces.[36,46]

In addition to investigating the effect of ferroelectric poling on water adsorption, we have examined the impact of water molecules on the surface with regard to both its structural (morphology) and electrostatic properties. Regarding the first, using the common surface roughness parameters R_a (arithmetic average of the absolute values) and R_q (root mean squared) as amplitude parameters,

$$R_a = \frac{1}{N}\sum_{i=1}^{n} |z_i|, \tag{7}$$

$$R_q = \sqrt{\frac{1}{N}\sum_{i=1}^{n} z_i^2}, \tag{8}$$

the calculated microscopic roughness of clean surfaces amounts to $R_a = 1.584$ Å, $R_q = 1.644$ Å for the positive and $R_a = 1.992$ Å, $R_q = 2.216$ Å for the negative surface, respectively. The surface roughness is also reflected by the differently corrugated charge densities at the two sides, as represented in Fig. 8. On both surfaces, the water adsorption accentuates the surface relaxation, proportionally to the amount of adsorbed molecules. Thus, the presence of a water film (water monolayer) increases the surface roughness to $R_a = 1.680$ Å, $R_q = 1.758$ Å for the positive and $R_a = 2.164$ Å, $R_q = 2.472$ Å for the negative surface. In the case of the negative LN(0001) surface, even the order of the outermost atomic layers changes. While oxygen forms the uppermost layer in vacuum, the Li atoms are pushed outward by nearly 1 Å upon adsorption of a complete water monolayer, so that they lie 0.06 Å above the oxygen atoms at the water-LN interface. Both the larger increase of the surface roughness as well as the change of order in the atomic layer can be traced back to the softer atomic bonds at the negative surface. These are demonstrated, in turn, by the softer phonon modes at the negative surface.[47]

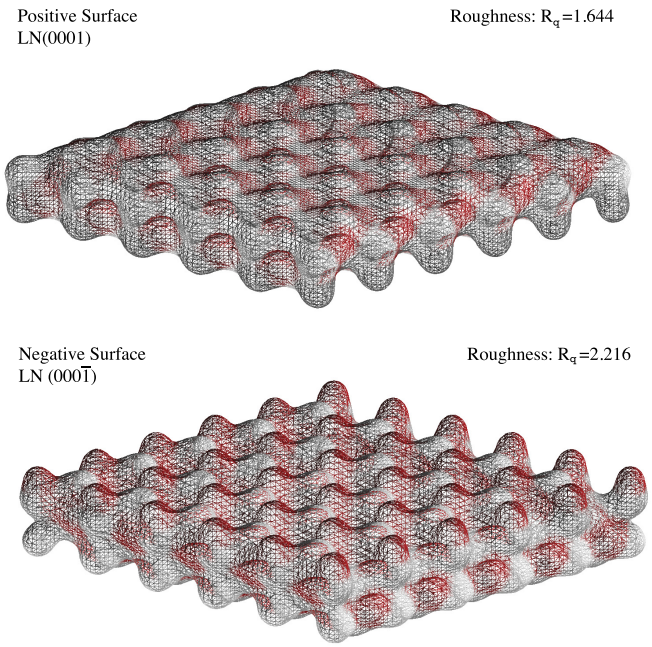

FIG. 8. (Color online) Charge density isosurface (0.01 $e/\text{Å}^3$) calculated for the clean positive (upper part) and negative (lower part) LN(0001) surface.

Regarding the electrostatics, the calculation of the work function upon adsorption yields insights into the charge compensation mechanisms, which play a crucial role in the physics of ferroelectric surfaces. Indeed, it allows us to determine the direction of the charge transfer between the surface and adsorbates. An estimation of the surface charge of ideal, relaxed surfaces can be found in Ref. 29. The authors present a simple electrostatic model, predicting a positive charge of $+e/4$ at the LN(000$\bar{1}$) (so called negative surface) and a negative charge of $-e/4$ at the LN(0001) (so called positive surface). This charge is expected to be compensated by adsorbates. We predict a decrease of the work function (of 0.34 eV) at the negative side and an increase of the work function (of 0.49 eV) at the positive side upon adsorption of a single molecule. This corresponds to an electron transfer directed from the molecule to the surface at the positively charged side and vice versa from the surface to the adsorbate at the negatively charged surface. Thus, the water adsorption has in both cases a stabilizing influence as it contributes to reduce the surface charge.

IV. CONCLUSIONS

We have performed density functional calculations to model the water adsorption at the $LiNbO_3$ surface. Isolated H_2O molecules are characterized by an adsorption energy of 0.61 and 1.28 eV at the positive and negative side, respectively. The adsorption configuration and adsorbate mobility are strongly polarization-dependent, in qualitative agreement with temperature programed desorption measurements.[11] This seems to be a general feature for the adsorption of polar molecules on the LN z surface, as revealed by recent experiments on the adsorption of 2-propanol on LN.[10] The adsorption energy differences are explained by different molecular bonding geometries on the two structurally distinct surfaces. With increasing water coverage, different structures are formed whose adsorption energy per molecule is in qualitative agreement with the TPD data. In further agreement with Ref. 11, the water adsorption is found to occur mainly nondissociatively, independently of the coverage. At ambient condition and assuming a relative humidity of 50%, we expect water molecules to be adsorbed at the LN(0001) surface, either in the form of thin films with honeycomb symmetry or in small clusters. The analysis of the vibrational frequencies of adsorbed water molecules may help to assess the occurring geometry for high coverage. Our calculations confirm that the water adsorption has a stabilizing effect on both the positive and negative $LiNbO_3$ surfaces.

ACKNOWLEDGMENTS

The calculations were done using grants of computer time from the Paderborn Center for Parallel Computing (PC^2) and the Höchstleistungs-Rechenzentrum Stuttgart (HLRS). The Deutsche Forschungsgemeinschaft is acknowledged for financial support.

*simone.sanna@uni-paderborn.de

[1] A. Räuber, *Chemistry and Physics of Lithium Niobate*, Current Topics in Materials Science (North-Holland, Amsterdam, 1978).
[2] R. S. Weis and T. K. Gaylord, Appl. Phys. A **37**, 191 (1985).
[3] K. Uchino, *Ferroelectric Devices*, 2nd ed. (CRC, Boca Raton, FL, 2009).
[4] G. Namkoong, K.-K. Lee, S. M. Madison, W. Henderson, S. E. Ralph, and W. A. Doolittle, Appl. Phys. Lett. **87**, 171107 (2005).
[5] Y. Watanabe, M. Okano, and A. Masuda, Phys. Rev. Lett. **86**, 332 (2001).
[6] W.-C. Yang, B. J. Rodriguez, A. Gruverman, and R. J. Nemanich, Appl. Phys. Lett. **85**, 2316 (2004).
[7] B. Rosenblum, P. Bräunlich, and J. P. Carrico, Appl. Phys. Lett. **25**, 17 (1974).
[8] K. Nassau, H. J. Levinstein, and G. M. Loiacono, J. Phys. Chem. Solids **27**, 983 (1966).
[9] C. L. Sones, S. Mailis, W. S. Brocklesby, R. W. Eason, and J. R. Owen, J. Mater. Chem. **295**, 12 (2002).
[10] Y. Yun, L. Kampschulte, M. Li, A. D. Liao, and E. I. Altman, J. Phys. Chem. C **111**, 13951 (2007).
[11] J. Garra, J. M. Vohs, and D. A. Bonnell, Surf. Sci. **603**, 1106 (2009).
[12] Y. Inoue, I. Yoshioka, and K. Sato, J. Phys. Chem. **88**, 1148 (1984).
[13] S. V. Kalinin, D. A. Bonnell, T. Alvarez, X. Lei, Z. Hu, J. H. Ferris, Q. Zhang, and S. Dunn, Nano Lett. **2**, 589 (2002).
[14] D. D. Fong, A. M. Kolpak, J. A. Eastman, S. K. Streiffer, P. H. Fuoss, G. B. Stephenson, C. Thompson, D. M. Kim, K. J. Choi, C. B. Eom, I. Grinberg, and A. M. Rappe, Phys. Rev. Lett. **96**, 127601 (2006).

[15]X. Liu, K. Kitamura, K. Terabe, H. Hatano, and N. Ohashi, Appl. Phys. Lett. **91**, 044101 (2007).
[16]S. Dunn and D. Tiwari, Appl. Phys. Lett. **93**, 092905 (2008).
[17]S. Habicht, R. J. Nemanich, and A. Gruveman, Nanotechnology **19**, 495303 (2008).
[18]D. Li, M. H. Zhao, J. Garra, A. M. Kolpak, A. M. Rappe, D. A. Bonnell, and J. M. Vohs, Nat. Mater. **7**, 473 (2008).
[19]S. C. Bharath, K. R. Pimputkar, A. M. Pronschinske, and T. P. Pearl, Appl. Surf. Sci. **254**, 2048 (2008).
[20]S. Rode, R. Hölscher, S. Sanna, S. Klassen, K. Kobayashi, H. Yamada, W. G. Schmidt, and A. Kühnle, Phys. Rev. B **86**, 075468 (2012).
[21]J. P. Perdew and Y. Wang, Phys. Rev. B **33**, 8800 (1986).
[22]G. Kresse and J. Furthmüller, Phys. Rev. B **54**, 11169 (1996).
[23]L. Giordano, J. Goniakowski, and J. Suzanne, Phys. Rev. Lett. **81**, 1271 (1998).
[24]W. G. Schmidt, M. Albrecht, S. Wippermann, S. Blankenburg, E. Rauls, F. Fuchs, C. Rödl, J. Furthmüller, and A. Hermann, Phys. Rev. B **77**, 035106 (2008).
[25]S. Sanna and W. G. Schmidt, Phys. Rev. B **81**, 214116 (2010).
[26]P. E. Blöchl, Phys. Rev. B **50**, 17953 (1994).
[27]A. Y. Lushkin, A. Y. Lushkin, V. B. Nazarenko, V. B. Nazarenko, K. N. Pilipchak, K. N. Pilipchak, V. F. Shnyukov, V. F. Shnyukov, A. G. Naumovets, and A. G. Naumovets, J. Phys. D **32**, 9 (1999).
[28]Y. Yun, M. Li, D. Liao, L. Kampschulte, and E. Altman, Surf. Sci. **601**, 4636 (2007).
[29]S. V. Levchenko and A. M. Rappe, Phys. Rev. Lett. **100**, 256101 (2008).
[30]H. Kawanowa, R. Souda, H. Ozawa, Y. Gotoh, K. Terabe, S. Takekawa, and K. Kitamura, Surf. Sci. Lett. **538**, L500 (2003).
[31]J. Neugebauer and M. Scheffler, Phys. Rev. B **46**, 16067 (1992).
[32]L. Bengtsson, Phys. Rev. B **59**, 12301 (1999).
[33]The sum of the ionic radii is 2.01 Å. www.webelements.com.
[34]P. Thissen, G. Grundmeier, S. Wippermann, and W. G. Schmidt, Phys. Rev. B **80**, 245403 (2009).
[35]A. Riefer, S. Sanna, and W. G. Schmidt, Phys. Rev. B **86**, 125410 (2012).
[36]S. Meng, E. G. Wang, and S. Gao, Phys. Rev. B **69**, 195404 (2004).
[37]A. Michaelides and K. Morgenstern, Nat. Mater. **6**, 597 (2007).
[38]O. Dulub, B. Meyer, and U. Diebold, Phys. Rev. Lett. **95**, 136101 (2005).
[39]F. Bechstedt, *Principle of Surface Physics*, Advanced Texts in Physics (Springer, Berlin, 2003).
[40]C. Thierfelder, A. Hermann, P. Schwerdtfeger, and W. G. Schmidt, Phys. Rev. B **74**, 045422 (2006).
[41]L. D. Landau and E. M. Lifshitz, *Statistical Physics, Part I*, 3rd ed. (Butterworth-Heinemann, Oxford, 1981).
[42]V. W. Laurie and D. R. Herschbach, J. Chem. Phys. **37**, 1687 (1962).
[43]F. Johann and E. Soergel, Appl. Phys. Lett. **95**, 232906 (2009).
[44]D. Ehre, E. Lavert, M. Lahav, and I. Lubomirsky, Science **327**, 672 (2010).
[45]R. Hölscher, S. Sanna, and W. G. Schmidt, Phys. Status Solidi C **9**, 1361 (2012).
[46]M. J. Stirniman, C. Huang, R. S. Smith, S. A. Joyce, and B. D. Kay, J. Chem. Phys. **105**, 1295 (1996).
[47]S. Sanna, G. Berth, W. Hahn, A. Widhalm, A. Zrenner, and W. G. Schmidt, IEEE Trans. Ultrason. Ferroelectr. Freq. Control **58**, 1751 (2011).